JACS
JOURNAL OF THE AMERICAN CHEMICAL SOCIETY

Anatolian University Libraries Consortium a·n·k·o·s

Subscriber access provided by ORTA DOGU TEKNIK UNIVERSITESI KUTUPHANESI

Article

Perfluorinated ligands induce *meridional* metal stereochemistry to generate ML, ML and ML prisms

Marion Kieffer, Ben S. Pilgrim, Tanya K Ronson, Derrick A. Roberts, Mina Aleksanyan, and Jonathan R. Nitschke

J. Am. Chem. Soc., **Just Accepted Manuscript** • DOI: 10.1021/jacs.6b02445 • Publication Date (Web): 04 May 2016

Downloaded from http://pubs.acs.org on May 4, 2016

Just Accepted

"Just Accepted" manuscripts have been peer-reviewed and accepted for publication. They are posted online prior to technical editing, formatting for publication and author proofing. The American Chemical Society provides "Just Accepted" as a free service to the research community to expedite the dissemination of scientific material as soon as possible after acceptance. "Just Accepted" manuscripts appear in full in PDF format accompanied by an HTML abstract. "Just Accepted" manuscripts have been fully peer reviewed, but should not be considered the official version of record. They are accessible to all readers and citable by the Digital Object Identifier (DOI®). "Just Accepted" is an optional service offered to authors. Therefore, the "Just Accepted" Web site may not include all articles that will be published in the journal. After a manuscript is technically edited and formatted, it will be removed from the "Just Accepted" Web site and published as an ASAP article. Note that technical editing may introduce minor changes to the manuscript text and/or graphics which could affect content, and all legal disclaimers and ethical guidelines that apply to the journal pertain. ACS cannot be held responsible for errors or consequences arising from the use of information contained in these "Just Accepted" manuscripts.

ACS Publications

Journal of the American Chemical Society is published by the American Chemical Society. 1155 Sixteenth Street N.W., Washington, DC 20036
Published by American Chemical Society. Copyright © American Chemical Society. However, no copyright claim is made to original U.S. Government works, or works produced by employees of any Commonwealth realm Crown government in the course of their duties.

Perfluorinated ligands induce *meridional* metal stereochemistry to generate M_8L_{12}, $M_{10}L_{15}$ and $M_{12}L_{18}$ prisms

Marion Kieffer, Ben S. Pilgrim, Tanya K. Ronson, Derrick A. Roberts, Mina Aleksanyan and Jonathan R. Nitschke*

Department of Chemistry, University of Cambridge, Lensfield Road, Cambridge CB2 1EW, United Kingdom

ABSTRACT: *Meridional* (*mer*) coordination promotes the generation of larger and lower-symmetry prismatic metallosupramolecular structures, in contrast with the *facial* (*fac*) coordination common to smaller and higher-symmetry polyhedra. Here we describe a general route to the selective formation of large metallosupramolecular prisms that contain exclusively *mer* coordinated metal vertices. The use of 2-formylpyridine subcomponents that contain perfluorophenylene substituents at their 5-positions resulted in stereoselective formation of the iron(II) complexes from these subcomponents. Only *mer* vertices were observed, as opposed to the statistical *fac*/*mer* mixture otherwise generated. This *mer*-selective self-assembly could be used to prepare tetragonal (M_8L_{12}), pentagonal ($M_{10}L_{15}$) and hexagonal ($M_{12}L_{18}$) prisms, by taking advantage of the subtle selectivities imposed by the different anilines and counterions employed. The equilibrium between the tetragonal and pentagonal prism followed a linear free energy relationship, with the ratio between structures correlating with the Hammett σ_p^+ parameter of the incorporated aniline. The contrasting preferences of the fluorinated and non-fluorinated ligands to generate prisms and tetrahedra respectively were quantified energetically, with the destabilization increasing linearly for each "incorrect ligand" incorporated into either structure.

INTRODUCTION

Recent advances in supramolecular chemistry have produced a host of intricate self-assembled architectures of increasing structural[1] and functional complexity.[2] As chemical self-assembly moves from an era of serendipity into one of rational design,[2e] elucidation of the rules that govern the assembly process becomes progressively more important. The structures of discrete metal-organic complexes that form in solution are determined by the geometric relationship between the coordination preferences of the metal and ligand components,[3] but also influenced by factors such as solvation,[4] concentration,[5] the ratio between components,[6] the presence of guests or templates,[7] and exposure to external stimuli such as light.[8] Directing the assembly of subcomponents into a desired structure requires control over the complex interplay between these factors.[9]

Homoleptic three-dimensional assemblies encompass structural types including the Platonic solids such as the tetrahedron,[10] cube[11] and icosahedron,[1f] and Archimedean solids such as the truncated tetrahedron,[12] cuboctahedron[13] and rhombicuboctahedron.[14] The formation of the simplest of these, the tetrahedron, is well precedented.[10] However, the selective formation of more complex, higher nuclearity structures is less common. Of these, the prismatic structures[15] are of particular interest, as they can feature well-defined cylindrical pores reminiscent of both natural[16] and synthetic ion channels.[17] However, there are few rules to guide the design of prismatic architectures with channels of varying dimensions. More robust rational design principles are therefore vital for realizing the potential applications of these self-assembled architectures.

Despite the similarity between the coordination vector relationships[18] required to form tetrahedra and prisms, the majority of bis-pyridylimine ligands investigated by our group assembled exclusively into tetrahedral structures when combined with octahedral metal centers.[19] The formation of prismatic architectures was observed only in specific solvent mixtures[4c] or in the presence of a templating anion.[20] Even then, these prisms in many cases existed in equilibrium with the corresponding tetrahedra. Tetrahedral structures are characterized by the *facial* (*fac*) coordination of these ligands (where the three imine nitrogen atoms define one triangular face of the octahedral coordination sphere),[21] whereas the prismatic structures possess *meridional* (*mer*) coordination (where the three imine nitrogen atoms define a plane that includes the metal center). Therefore, we postulated that the use of ligands that exhibit a clear preference for the formation of *mer* vertices would facilitate the selective formation of novel prismatic architectures over the more frequently-observed tetrahedra. Hence, we set out to explore factors responsible for generating *mer* coordination in transition metal complexes that incorporate the versatile 2-pyridylimine ligand motif.

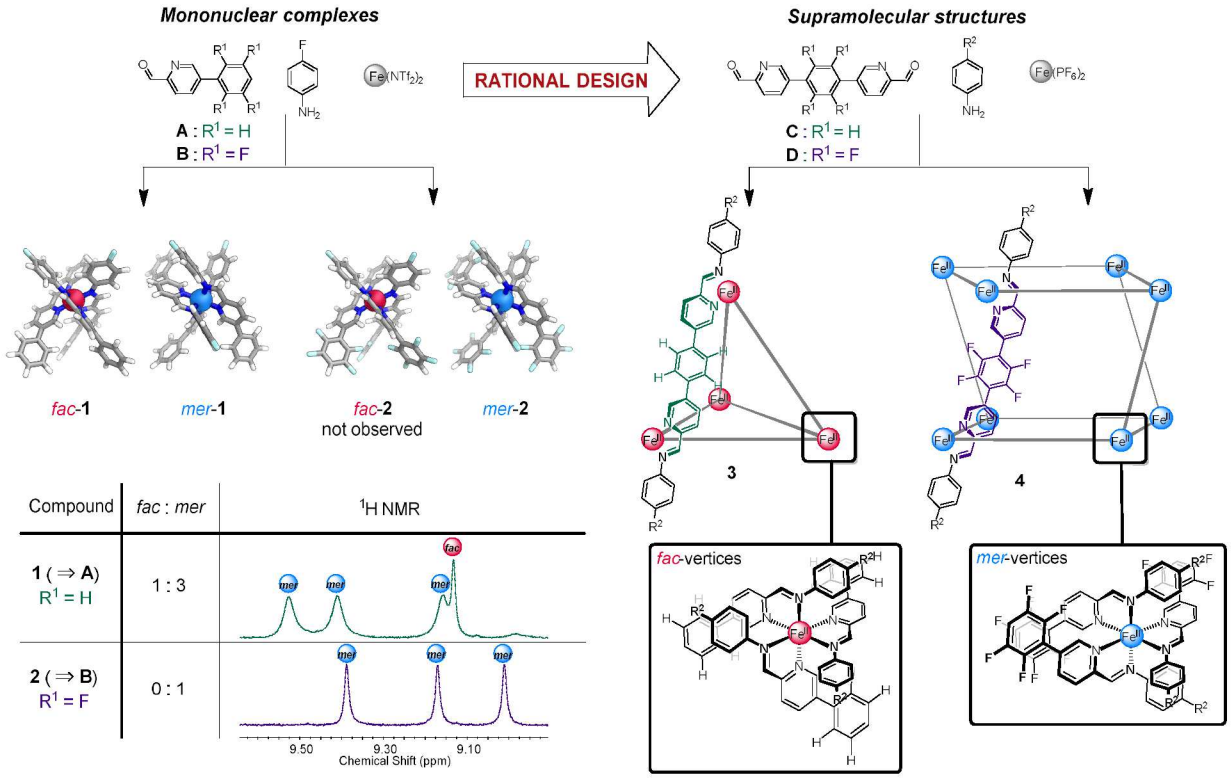

Figure 1. Self-assembly of *fac* and *mer* mononuclear complexes **1** and **2**. ^{1}H NMR spectra (400 MHz, 298 K, CD_3CN) of the imine regions of **1** and **2**. Self-assembly of tetrahedral **3** and tetragonal prismatic **4** from the non-fluorinated **C** and tetrafluorinated **D** subcomponents respectively.

RESULTS AND DISCUSSION

Rational Design of Prismatic Structures. In order to elucidate structural preferences that would favor the formation of *mer* vertices over *fac*, we scrutinized several previously obtained crystal structures. Around the *fac* vertices in these structures,[22] substituents on the aromatic rings attached to the 5-positions of the pyridine rings experienced a more sterically crowded environment than in the corresponding *mer* vertices.[20] Furthermore, the sizes and positions of the ligand substituents have been shown to influence the product stereochemistry.[23] We thus postulated that by making the aromatic substituent at the 5-position on the pyridine rings more sterically demanding, the formation of *fac* vertices might be disfavored relative to *mer*, as illustrated in the van der Waals space filling models and surfaces provided in Supporting Information (SI) Section S2.1. *Mer* vertices also provide greater potential for π-stacking interactions between the electron-rich aniline ring and the electron deficient pyridine ring as shown in Figure 1 and in the Electrostatic Potential Map (SI, Section S2.2). Consequently, adding electron-withdrawing substituents to the pyridine ring should enhance these quadrupolar interactions and favor the formation of *mer* vertices. By replacing the benzene ring linking the two pyridine rings with a 2,3,5,6-tetrafluorobenzene ring, we inferred that both of these requirements could be fulfilled due to the slightly larger van der Waals radius of fluorine (1.47 Å) compared to hydrogen (1.00 Å),[24] and the electron-withdrawing nature of the fluorine atoms.

In order to test this hypothesis, we first synthesized a pair of mononuclear model complexes and examined the ratio of *fac* to *mer* isomers (Figure 1). The subcomponent self-assembly[25] of 2-formyl-5-phenylpyridine **A**, with *p*-fluoroaniline and iron(II) bis(trifluoromethane)sulfonimide ($Fe(NTf_2)_2$) in CH_3CN furnished mononuclear complex **1** (Figure 1). ESI-MS results were consistent with the expected formation of complexes of $Fe^{II}L_3$ stoichiometry. ^{1}H NMR analysis indicated the presence of both *fac* and *mer* geometries in the statistical proportion of 1:3. In contrast, the self-assembly of the fluorinated 2-formyl-5-(2,3,5,6-tetrafluorophenyl)pyridine **B**, with *p*-fluoroaniline and $Fe(NTf_2)_2$, produced mononuclear complex **2** possessing exclusively *mer* geometry, as indicated by ^{1}H NMR.

As the model compound studies supported our hypothesized method of stereocontrol, we then embarked on the synthesis of the appropriate bis-formylpyridine subcomponents to assemble into the desired larger structures. As previously reported,[22a] the self-assembly of dialdehyde subcomponent **C** with *p*-methoxyaniline and iron(II) hexafluorophosphate ($Fe(PF_6)_2$) gave tetrahedral cage **3** in solution. In order to access the desired prismatic structures, dialdehyde subcomponent **D**, which contains a 2,3,5,6-tetrafluorobenzene moiety bridging the two for-

mylpyridine groups, was required. Dialdehyde **D** was synthesized in four steps, as described in the Supporting Information (SI), Section S1.2.1. The self-assembly of **D** with *p*-methoxyaniline and $Fe(PF_6)_2$ gave rise to a product having the formula $Fe^{II}_8L_{12}$ by ESI-MS (SI, Figure S27). The ^{1}H NMR spectrum revealed the presence of a predominant species with three magnetically distinct ligand environments, consistent with tetragonal prismatic structure **4a** (R^2=OMe) with *mer* coordination at all vertices (Figure 1).

Slow vapor diffusion of benzene into an acetonitrile solution of **4a** afforded a crystal suitable for X-ray diffraction analysis, which confirmed the tetragonal prismatic structure of the assembly. The complex consists of two four-sided circular helicate rings, each made of four iron(II) centers linked by four equatorial ligands. The two rings are bridged by four axial ligands (Figure 2) with a twist of 15° between the two parallel rings. The metal-to-metal distances are 12.0 Å within the $Fe^{II}_4L_4$ rings and 11.8 Å between rings. All metal centers in each structure possess the same *Δ* or *Λ* handedness, giving the structure idealized D_4 point symmetry. Both enantiomeric forms of **4a** were present in the crystal. Although Ward has isolated a stereochemically similar all-*mer meso* M_8L_{12} structure,[11a] and other M_8L_{12} structures have been reported displaying different combinations of *fac* and *mer* vertices,[11a,26] the chirality and stereochemical configuration of **4** generate a new structure type, to the best of our knowledge.

The crystal structure also revealed the presence of ordered PF_6^- counterions in the partially enclosed triangular pockets in the top and bottom rings. Two more PF_6^- ions occupy the central channel, disordered around the C_4 symmetry axis. The position of the PF_6^- ions in the triangular pockets, and the distance of these anions from the aromatic rings of the ligands, suggested the presence of significant anion-π interactions[27] in the solid state. The presence of these interactions in the solution phase was also inferred by the observed broadening and downfield shifting (by 0.23 ppm) of the PF_6^- doublet in the ^{19}F NMR spectrum (SI, Figure S70).

Although the solid-state structure of **4a** suggests that included PF_6^- anions play a structural role, the difference in behavior of fluorinated building block **D** with respect to its non-fluorinated analog **C** is not only due to the presence of PF_6^- anions, as evidenced by the formation of tetrahedral cage **3** (*fac* vertices only) under identical conditions, when subcomponent **C** was employed in place of **D**. We infer the perfluorophenylene-derived stereoselectivity observed during this self-assembly process to originate from the same factors that led to different stereochemical outcomes between model compounds **1** and **2** (Figure 1).

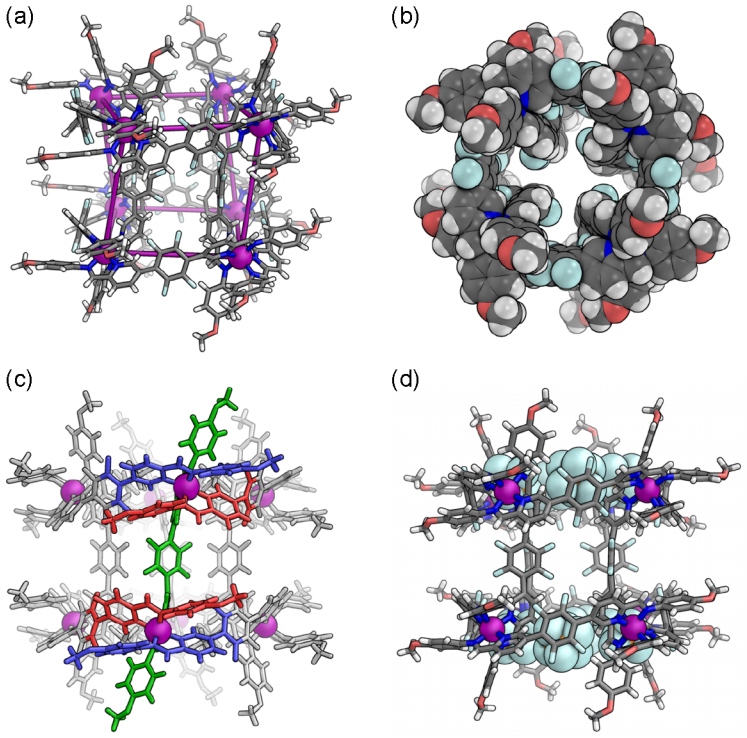

Figure 2. Views of the single crystal X-ray structure of **4a** (a) showing the top and bottom rings linked by axial ligands, with linkages between Fe^{II} centers (purple spheres) added in order to highlight the D_4 point symmetry; (b) showing the ligands in a space-filling view down the central channel; (c) highlighting a pair of *mer* vertices, with the three magnetically distinct environments shown in blue, red, and green; (d) showing the placement of the ordered PF_6^- counterions above the -C_6F_4- rings. In all views the non-encapsulated anions, solvent molecules and disorder are omitted for clarity.

The contrasting preference of subcomponents **C** and **D** to form only tetrahedral or prismatic structures respectively was probed further in experiments employing mixtures of the two subcomponents. As both subcomponents have nearly identical lengths, we expected them to mix to form a library of heteroleptic assemblies if neither ligand had a distinct preference for either structural type. If mixed in equal amounts, a deviation from the entropically-favored statistical (binomial) distribution of heteroleptic assemblies, even in the absence of complete narcissistic self-sorting,[28] would indicate an inherent preference for the ligands to self-sort into their preferred structural type.

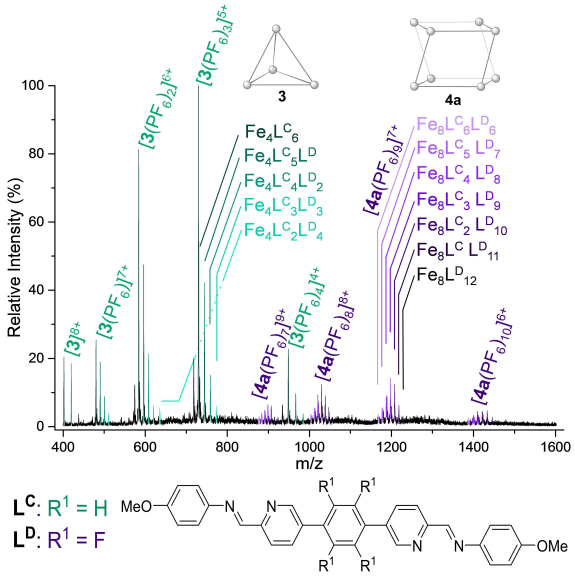

Figure 3. ESI-MS of a mixture of preformed structures **3** and **4a** in a 2:1 ratio after equilibration at 50 °C for one week.

Tetrahedral cage **3** and tetragonal prism **4a** were combined in a 2:1 ratio, giving a 1:1 ratio between the non-fluorinated subcomponent **C** and fluorinated subcomponent **D** within the sample. The mixture was left to equilibrate at 50 °C for one week. The ^{1}H NMR spectrum of the mixture became significantly more complex during this time, but did not change further, indicating that the system had reached equilibrium.

ESI-MS results (Figure 3) indicated the presence of $Fe^{II}_4L_6$ tetrahedra incorporating between zero and four fluorinated **D** residues, but no tetrahedra incorporating five or six. Peaks corresponding to $Fe^{II}_8L_{12}$ tetragonal prisms incorporating between zero and six non-fluorinated **C** residues were also observed, but none incorporating more than six. Hence, a clear deviation from the binomial distribution was obtained across both architectures. The intractability of the ^{1}H NMR spectrum was thus inferred to result both from the many different congeners present, and the different structural arrangements that may be adopted by some congeners (e.g. $Fe_4L^c_4L^D_2$).

We infer that when observing clusters of ESI-MS peaks, where all signals correspond to structures with a common structure type – either tetrahedra (**3**) or tetragonal prisms (**4**) – in a single charge state, the response factors (peak intensities) were independent of the number of fluorinated ligands present in each tetrahedron, or which structural isomer was present. Thus, the concentration of each of the congeners was considered to be proportional to the intensity of its *m*/*z* peak, and the relative proportions of species differing only in the number of fluorinated ligands incorporated were determined by measuring the differences in peak intensities. This method has provided consistent results in the context of other complex metallosupramolecular architectures.[29]

Within each charge state, the intensities of the *m*/*z* peaks were normalized, and these intensities were averaged across all observed charge states to give the relative amounts of each congener in solution. These values were plotted alongside the binomial distribution (Figure 4a). In the cases of both tetrahedra (**3**) and tetragonal prisms (**4**), strong deviations were observed from binomial distributions of products that incorporate both kinds of ligands (Figures 4a and 4b, respectively). These deviations reflected the energetic preference of non-fluorinated subcomponent **C** to form tetrahedron **3** and fluorinated subcomponent **D** to form tetragonal prism **4a**.

In order to quantify these energetic preferences, a set of equilibrium constants were calculated between congeners in the tetrahedral series, by measuring the ratio between the observed proportion of each species and its expected proportion, based upon a binomial distribution (SI, Section S4.3 for details). The relative energies between congeners were determined from these equilibrium constants. These Gibbs energies were plotted relative to the baseline of fully non-fluorinated tetrahedral cage **3,** which was destabilized by an average of 4.1 kJ mol^{-1} for each fluorinated subcomponent **D** incorporated into the tetrahedral cage, as determined by a linear least-squares fit (Figure 4c). We cannot differentiate between structural isomers *via* ESI-MS, therefore only a weighted average energy was calculated. Applying the same procedure to the tetragonal prism **4a** indicated that the incorporation of each non-fluorinated subcomponent **C** incurred an average energetic destabilization of 2.7 kJ mol^{-1}.

It is thus more energetically costly to incorporate a fluorinated ligand into a tetrahedron than a non-fluorinated ligand into a tetragonal prism, which is consistent with the observation that mononuclear complex **1** formed as a statistical *fac*-*mer* mixture, whereas *mer*-**2** formed stereoselectively. The relative contributions of entropy and enthalpy to the tetrahedron-prism equilibria cannot be quantified based upon the data available, and a meaningful van 't Hoff analysis is precluded by the slowness of equilibration below 50 °C, and broadening of the ^{1}H NMR spectrum, consistent with possible sample degradation, above 70 °C. Entropy tends to favors the formation of structures with the minimum number of components[3a,5a] and in this case the tetrahedron incorporates half the number of building blocks than the prism. Given that the non-fluorinated mononuclear complex **1** has no preference for *fac* or *mer* geometry, entropy might be

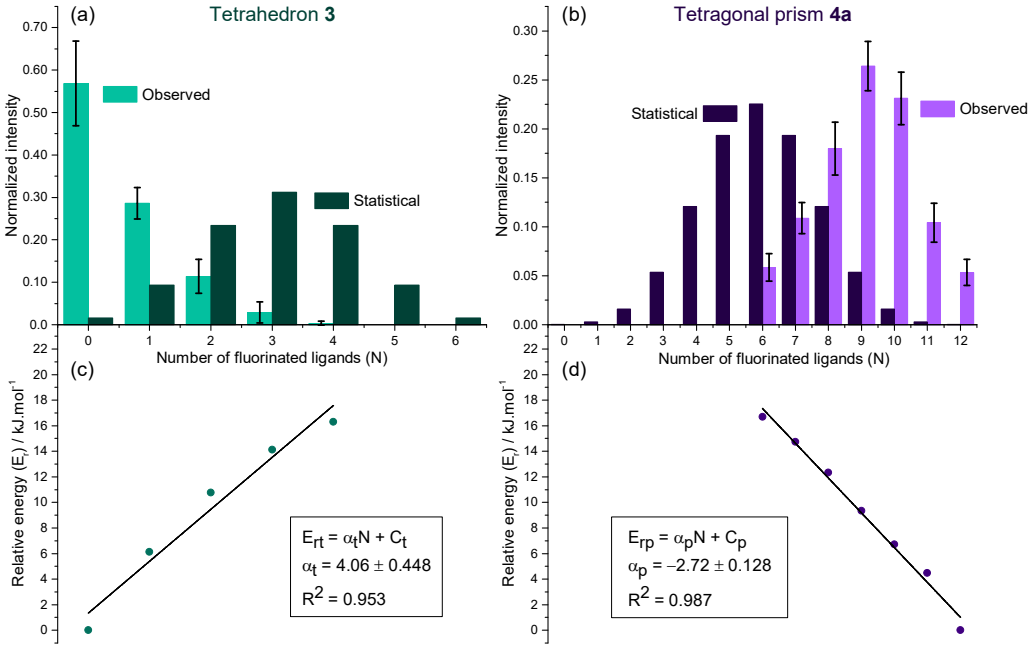

Figure 4. Proportion of each species observed for (a) tetrahedron **3** and (b) tetragonal prism **4a** compared to the binomial (statistical) distribution. Error bars represent the standard deviations of the amounts of each congener measured between the different charge states observed in the ESI-MS. (c) and (d) provide plots of the energy of each species relative to tetrahedron **3** in (c), containing only non-fluorinated **C** residues, and the tetragonal prism **4a** in (d), containing only fluorinated **D** residues. E_{rt} and E_{rp} refer to the relative energies between congeners respectively in the cases of the tetrahedral series and the prismatic series. α represents the energetic destabilization per ligand exchanged.

driving the preference of the non-fluorinated ligand to form the tetrahedron. The observation of the larger prismatic structures formed from fluorinated ligands suggests that prisms are enthalpically favored, outweighing the entropic preference to form tetrahedra.

When the self-assembly reaction was performed using equal amounts of subcomponents **C** and **D**, the same result was obtained as for when the preformed cages were mixed together, indicating that the thermodynamic product distribution was attained in both cases.

Formation of larger prismatic structures. Tetragonal prism **4a** was the predominant species obtained in solution from the self-assembly reaction of dialdehyde **D** with *p*-methoxyaniline and $Fe(PF_6)_2$, as determined by ^{1}H NMR. Notably, signals attributable to a $Fe^{II}_4L_6$ tetrahedral cage were absent from the ^{1}H NMR spectrum. However, the observation of minor peaks indicated the presence of another discrete supramolecular species in solution.

Given the propensity of subcomponent **D** to form structures containing *mer* vertices, we hypothesized that the additional ^{1}H NMR signals might be due to higher-order prismatic structures. The optimum prism size could be the result of a balance between increased strain in smaller structures and the entropic penalty of forming larger structures, with various factors and effects having the potential to tip this balance, as described below.

Previous work has shown that counter-anions can influence the product distributions of self-assembly reactions due to their templating effects.[26] We inferred that anion templation might play a role in determining the predominant product, based on the interactions observed between tetragonal prism **4a** and PF_6^- both in solution and in the solid state, as noted above. It has also been shown that the aniline subcomponent may influence the behavior of a structure in solution, due to delocalization of electron density between the aniline residue and the rest of the ligand.[30] Different combinations of anilines and counter anions were therefore screened in order to target the larger prismatic homologues of **4**.

The self-assembly of **D**, *p*-*tert*-butylaniline and iron(II) perchlorate gave a mixture of two species in the ^{1}H NMR spectrum, both having three distinct ligand environments, consistent with the presence of two prismatic structures. ESI-MS peaks were observed corresponding to both $Fe^{II}_8L_{12}$ (**4b**) and $Fe^{II}_{10}L_{15}$ (**5b**) structures (Figure 5a). Intriguingly, when **D** was mixed with *p*-methoxyaniline and $Fe(NTf_2)_2$, the ^{1}H NMR spectrum again indicated the formation of two predominant species; however, in contrast to the results with *p*-*tert*-butylaniline, ESI-MS gave results consistent with the presence of both $Fe^{II}_{10}L_{15}$ (**5a**) and $Fe^{II}_{12}L_{18}$ structures (**6a**) (Figure 5b).

Crystals were obtained following slow vapor diffusion of benzene into the mixture of **5c** and **6c**, formed from the reaction of **D** with *p*-fluoroaniline and $Fe(NTf_2)_2$ in

CH_3CN to which NBu_4PF_6 (ca. 30 equivalents per cage) had been added. Single-crystal X-ray diffraction afforded the structure shown in Figure 6, confirming the presence of a $Fe^{II}_{10}L_{15}$ pentagonal prism. The structure consisted of two parallel pentagonal circular helicate rings, each containing five equatorial ligands and five iron(II) centers. These parallel rings were linked by five axial ligands (Figure 6).

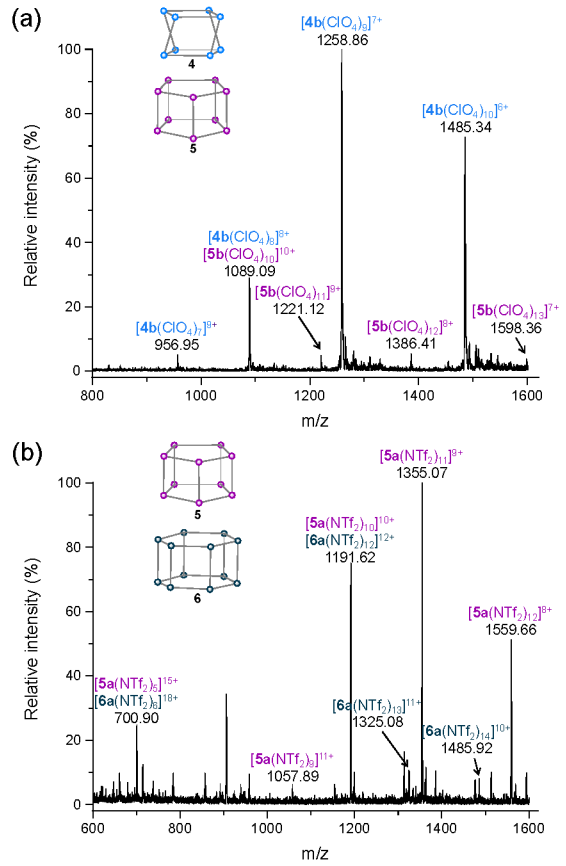

Figure 5. ESI-MS of a mixture of (a) **4b** and **5b** and (b) **5a** and **6a.**

The metal-to-metal distances are 12.3-13.2 Å within the $Fe^{II}_5L_5$ rings and 11.4-12.1 Å between rings. As with **4**, all vertices possessed *mer* stereochemistry, but remarkably, each structure contained metal centers of both Δ and *Λ* handedness. Within one complex, one pentagonal face contained five centers of Δ handedness and the other pentagonal face five centers of *Λ* handedness. The idealized structure of the assembly thus possesses a C_5 axis down the prism channel and a horizontal mirror plane through the center of the structure perpendicular to this axis, giving it C_{5h} point symmetry. This achiral structure contrasts with the chiral pentagonal prisms observed previously that contained metal centers of only one handedness in all cases.[4c,20] Similar to the structure of **4a**, PF_6^- counterions are found in partially-enclosed pockets within the top and bottom pentagonal rings (Figure 6c); however, several of the anions were disordered and/or modeled with partial occupancy. The limited resolution of the X-ray data prevented more detailed comparisons from being drawn between the structures of **4a** and **5c**. A crystal structure of **5a** having the same symmetry (C_{5h}) was obtained following the self-assembly of **D** with *p*-methoxyaniline and $Fe(NTf_2)_2$ in acetonitrile to which $K_2B_{12}F_{12}$ (ca. 40 equivalents per cage) had been added (SI, Figure S95). Some disordered $B_{12}F_{12}^{2-}$ counterions were also found in the pockets of this structure.

The differing symmetries of chiral M_8L_{12} **4a** and achiral $M_{10}L_{15}$ **5a** were maintained in the solution state, as indicated by experiments in which the chiral anion Δ-TRISPHAT[31] was added to the two prisms. Upon addition of Δ-TRISPHAT to mixtures of **4** and **5** (one equivalent of Δ-TRISPHAT per 8 Fe^{II}), only one of the two sets of signals was observed to split (SI, Section S5.1), as would be expected during the formation of diastereomeric ion pairs for chiral **4**, but not for achiral **5**. This experiment also confirmed unambiguously our assignments of the different signals to **4** and **5**, allowing quantification of the relative amounts of these species observed in the mixtures from ^{1}H NMR data.

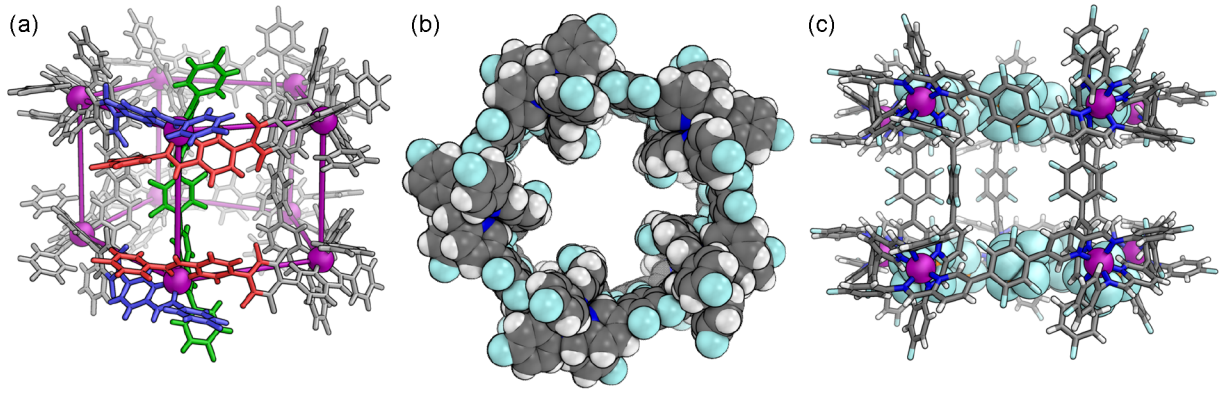

Figure 6. Single crystal X-ray structure of **5c** showing (a) the two pentagonal faces linked by axial ligands, with connections between metal centers (purple spheres) added to highlight the C_{5h} point symmetry; (b) spacefilling view down the central channel; (c) side view showing the specific positions of the localized PF_6^- counterions. In all views the non-encapsulated anions, solvent molecules and disorder are omitted for clarity.

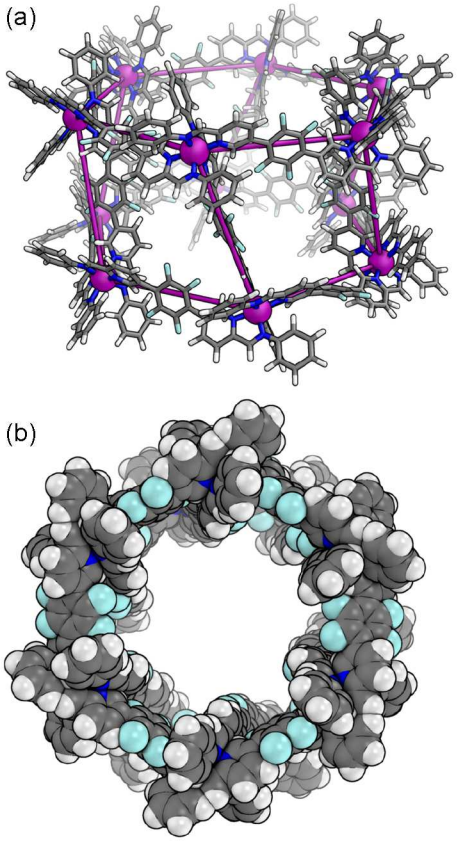

Figure 7. (a) MM3-optimized molecular model of hexagonal prism **6h** (R=H). Conections between metal centers (purple spheres) have been added to highlight the D_6 point symmetry; (b) spacefilling view down the central channel. No anions were modeled.

Upon addition of Δ-TRISPHAT (two equivalents per 10 Fe^{II}) to mixtures of **5** and **6**, the signals for **6** were observed to split in the ^{1}H NMR (SI, Section S5.2), consistent with a chiral $M_{12}L_{18}$ architecture possessing idealized D_6 point symmetry.

Despite many attempts, crystals of **6** suitable for X-ray diffraction analysis were not obtained. An MM3 model of **6** was constructed based on the proposed structure from the solution experiments (Figure 7). Between each architecture the increase in diameter of the central channel was substantial, expanding from 4.5 Å to 9.5 Å and 15.1 Å at the narrowest points of the channels for the tetragonal **4**, pentagonal **5** and hexagonal **6** prisms respectively.

The electronic influence of peripheral aniline substituents upon supramolecular architectures formed in solution is an area of current interest.[32] A more electron-rich aniline motif (as quantified by the Hammett σ_p parameter[33] of its substituent) leads to stronger metal-ligand interactions, in turn generating more stable structures. Hence, more electron-rich anilines are observed to displace less electron-rich anilines from a complex. However, the influence of the aniline substituent can extend well beyond the metal center itself.[30]

We thus sought a correlation between the electron withdrawing or donating ability of the aniline substituent and the relative stabilities of the prismatic structures described herein. Anilines bearing substituents with varying electronic effects were combined with subcomponent **D** and $Fe(PF_6)_2$. This iron(II) salt was chosen because ESI-MS and ^{1}H NMR indicated that it led to the formation of a mixture of two structures only (**4** and **5**) (Figure 8).

A weak linear free energy relationship was observed between the logarithm of the equilibrium constant for the interconversion of **4** and **5** (log K) and σ_p, (SI, Figure S92). By contrast, we noted a much stronger linear correlation between log K and the Hammett σ^+_p parameter, which takes resonance effects into account (Figure 8). We attribute the higher quality of this fit to the importance of direct electronic conjugation between the pyridine nitrogen atom and the aniline substituent. The sensitivity of the **4** ⇌ **5** equilibrium to electronic effects, as reported by the magnitude of the Hammett ρ value of 3.56, reflects the high degree of predictive control over the system's product distribution achievable by varying the aniline substituents.

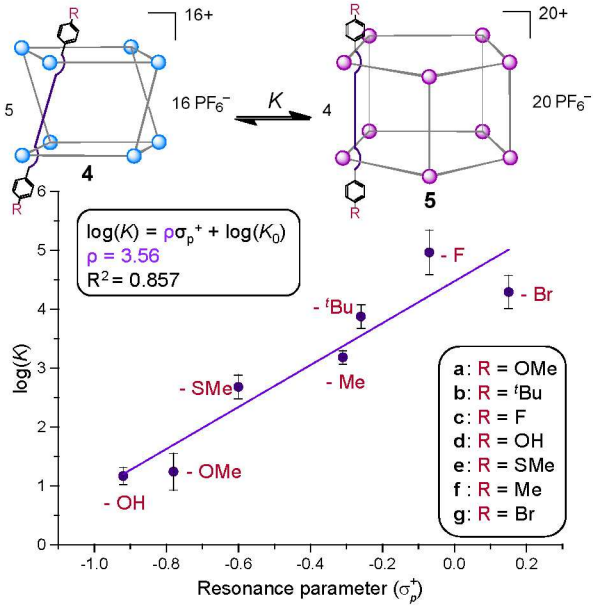

Figure 8. Equilibria between **4** and **5** show a linear free energy relationship between log(K) and σ_p^+, following the Hammett Equation. The error bars show standard deviations of log(K) over 5 runs.

We infer tetragonal prism **4** to be entropically favored with respect to pentagonal prism **5**, because **4** incorporates fewer of the same building blocks. Examination of the angle between the pyridine-tetrafluorobenzene-pyridine ring centroids in the crystal structures of prisms **4a** and **5c** revealed angles of 172° in prism **4a** and of 173-178° in prism **5c**, indicating that the ligands of tetragonal **4** are bent to a greater degree, and therefore more

strained, than the ligands of pentagonal **5**. No statistically significant differences in interligand π-π stacking were observed between the structures of **4a** and **5c**. Hence, pentagonal prism **5** should be favored on enthalpic grounds.[5a] We thus infer that the stronger metal-ligand interactions that result from the incorporation of more electron-rich anilines are needed to stabilize the more highly-strained tetragonal prismatic structure **4**. The strength of the metal-ligand interaction, as influenced by the substituents of the aniline residues, thus impacts strongly upon the equilibrium between these prismatic structures.

CONCLUSION

Although great strides have been made towards the rational design of supramolecular structures in recent years, many subtle factors require a greater degree of understanding before concepts of retrosynthetic analysis[34] can be as readily applied to these metal-organic assemblies as to purely organic molecules. This work elucidates key factors that lead a bidentate ligand to form *mer* rather than *fac* metal vertices—a salient feature of more structurally complex assemblies—which may in turn lead to more complex functions. The prismatic structures formed selectively during the course of this study might embed in membranes and act as channels to gate passage of small molecules or ions.[35] To realize this potential, both channel pore size and channel length must be controlled.

This study reports the synthesis of one of the largest prismatic architectures prepared to date, and reveals how the relative amounts of tetragonal and pentagonal prisms can be quantitatively controlled using the Hammett equation. We have also quantified the energetic preference of fluorinated ligands to form *mer* vertices, and therefore prismatic structures, finding it greater than the preference of non-fluorinated ligands to generate *fac* vertices and thus tetrahedra. The formation of larger hexagonal prisms could also be favored through variation of the counter anion. We aim next to explore the functions of these new structures, and to apply these lessons to the construction of yet more structurally complex supramolecular architectures incorporating *mer* stereocenters.

ASSOCIATED CONTENT

Supporting Information. Synthetic procedures and characterization of subcomponents **A**, **B** and **D**, characterization of complexes **1**, **2**, **4**, **5** and **6**, spectroscopic data, energetic modeling of **1** and **2,** evidence of anion-π interactions, details of mixed ligand experiments, Δ-TRISPHAT addition, Hammett studies and the CIF file for **4** and **5**. This material is available free of charge via the Internet at http://pubs.acs.org. Crystallographic data have been deposited with the Cambridge Crystallographic Data Centre as entries CCDC 1442988-1442991.

AUTHOR INFORMATION

Corresponding Author

*jrn34@cam.ac.uk

Notes

The authors declare no competing financial interest.

ACKNOWLEDGEMENT

This project has received funding from the European Union's Horizon 2020 research and innovation programme under the Marie Sklodowska-Curie grant agreement No 642192 and was supported by the UK Engineering and Physical Sciences Research Council (EPSRC). The authors thank Diamond Light Source (UK) for synchrotron beamtime on I19 (MT8464 and MT11397), the Department of Chemistry NMR facility, University of Cambridge, and the EPSRC UK National Mass Spectrometry Facility at Swansea University. M.K. acknowledges the Cambridge Commonwealth, European and International Trust and the Frédéric Fontaine scholarship from Michelin SCA. B.S.P. acknowledges the Herchel Smith Research Fellowship from the University of Cambridge and a Fellowship from Corpus Christi College, Cambridge. D.A.R. acknowledges the Gates Cambridge Trust for Ph.D. funding.

REFERENCES

(1) (a) Ayme, J.-F.; Beves, J. E.; Leigh, D. A.; McBurney, R. T.; Rissanen, K.; Schultz, D. *Nat. Chem.* **2012**, *4*, 15-20; (b) Chichak, K. S.; Cantrill, S. J.; Pease, A. R.; Chiu, S.-H.; Cave, G. W. V.; Atwood, J. L.; Stoddart, J. F. *Science* **2004**, *304*, 1308-1312; (c) Beves, J. E.; Blight, B. A.; Campbell, C. J.; Leigh, D. A.; McBurney, R. T. *Angew. Chem. Int. Ed.* **2011**, *50*, 9260-9327; (d) Forgan, R. S.; Sauvage, J.-P.; Stoddart, J. F. *Chem. Rev.* **2011**, *111*, 5434-5464; (e) Ward, M. D. *Chem. Commun.* **2009**, 4487-4499; (f) Pasquale, S.; Sattin, S.; Escudero-Adán, E. C.; Martínez-Belmonte, M.; de Mendoza, J. *Nat. Commun.* **2012**, *3*, 785; (g) Sun, B.; Wang, M.; Lou, Z.; Huang, M.; Xu, C.; Li, X.; Chen, L.-J.; Yu, Y.; Davis, G. L.; Xu, B.; Yang, H.-B.; Li, X. *J. Am. Chem. Soc.* **2015**, *137*, 1556-1564.

(2) (a) Heinrich, T.; Traulsen, C. H. H.; Holzweber, M.; Richter, S.; Kunz, V.; Kastner, S. K.; Krabbenborg, S. O.; Huskens, J.; Unger, W. E. S.; Schalley, C. A. *J. Am. Chem. Soc.* **2015**, *137*, 4382-4390; (b) Mauro, M.; Aliprandi, A.; Septiadi, D.; Kehr, N. S.; De Cola, L. *Chem. Soc. Rev.* **2014**, *43*, 4144-4166; (c) Yoon, H. J.; Kuwabara, J.; Kim, J.-H.; Mirkin, C. A. *Science* **2010**, *330*, 66-69; (d) Cook, T. R.; Vajpayee, V.; Lee, M. H.; Stang, P. J.; Chi, K.-W. *Acc. Chem. Res.* **2013**, *46*, 2464-2474; (e) Faulkner, A. D.; Kaner, R. A.; AbdallahQasem, M. A.; Clarkson, G.; Fox, D. J.; Gurnani, P.; Howson, S. E.; Phillips, R. M.; Roper, D. I.; Simpson, D. H.; Scott, P. *Nat. Chem.* **2014**, *6*, 797-803; (f) Chan, A. K.-W.; Lam, W. H.; Tanaka, Y.; Wong, K. M.-C.; Yam, V. W.-W. *Proc. Nat. Acad. Sci.* **2015**, *112*, 690-695; (g) Tatum, L. A.; Su, X.; Aprahamian, I. *Acc.*

Chem. Res. **2014**, *47*, 2141-2149; (h) Lee, H. Y.; Song, X.; Park, H.; Baik, M.-H.; Lee, D. *J. Am. Chem. Soc.* **2010**, *132*, 12133-12144; (i) Zhang, Z.; Kim, D. S.; Lin, C.-Y.; Zhang, H.; Lammer, A. D.; Lynch, V. M.; Popov, I.; Miljanić, O. Š.; Anslyn, E. V.; Sessler, J. L. *J. Am. Chem. Soc.* **2015**, *137*, 7769-7774.

(3) (a) Chakrabarty, R.; Mukherjee, P. S.; Stang, P. J. *Chem. Rev.* **2011**, *111*, 6810-6918; (b) Fujita, M.; Tominaga, M.; Hori, A.; Therrien, B. *Acc. Chem. Res.* **2005**, *38*, 369-378.

(4) (a) Kilbas, B.; Mirtschin, S.; Scopelliti, R.; Severin, K. *Chem. Sci.* **2012**, *3*, 701-704; (b) Suzuki, K.; Kawano, M.; Fujita, M. *Angew. Chem. Int. Ed.* **2007**, *46*, 2819-2822; (c) Zarra, S.; Clegg, J. K.; Nitschke, J. R. *Angew. Chem. Int. Ed.* **2013**, *52*, 4837-4840.

(5) (a) Weilandt, T.; Troff, R. W.; Saxell, H.; Rissanen, K.; Schalley, C. A. *Inorg. Chem.* **2008**, *47*, 7588-7598; (b) Kraus, T.; Buděšínský, M.; Cvačka, J.; Sauvage, J.-P. *Angew. Chem. Int. Ed.* **2006**, *45*, 258-261; (c) Yamamoto, T.; Arif, A. M.; Stang, P. J. *J. Am. Chem. Soc.* **2003**, *125*, 12309-12317; (d) Fu, J.-H.; Lee, Y.-H.; He, Y.-J.; Chan, Y.-T. *Angew. Chem. Int. Ed.* **2015**, *54*, 6231-6235; (e) Fujita, M.; Sasaki, O.; Mitsuhashi, T.; Fujita, T.; Yazaki, J.; Yamaguchi, K.; Ogura, K. *Chem. Commun.* **1996**, 1535-1536.

(6) (a) Sun, Q.-F.; Sato, S.; Fujita, M. *Nat. Chem.* **2012**, *4*, 330-333; (b) Kishi, N.; Akita, M.; Yoshizawa, M. *Angew. Chem. Int. Ed.* **2014**, *53*, 3604-3607; (c) Carnes, M. E.; Collins, M. S.; Johnson, D. W. *Chem. Soc. Rev.* **2014**, *43*, 1825-1834.

(7) (a) Freye, S.; Michel, R.; Stalke, D.; Pawliczek, M.; Frauendorf, H.; Clever, G. H. *J. Am. Chem. Soc.* **2013**, *135*, 8476-8479; (b) Scherer, M.; Caulder, D. L.; Johnson, D. W.; Raymond, K. N. *Angew. Chem. Int. Ed.* **1999**, *38*, 1587-1592; (c) Peng, R.; Li, D.; Wu, T.; Zhou, X.-P.; Ng, S. W. *Inorg. Chem.* **2006**, *45*, 4035-4046; (d) Custelcean, R. *Chem. Soc. Rev.* **2014**, *43*, 1813-1824.

(8) (a) Yan, X.; Xu, J.-F.; Cook, T. R.; Huang, F.; Yang, Q.-Z.; Tung, C.-H.; Stang, P. J. *Proc. Nat. Acad. Sci.* **2014**, *111*, 8717-8722; (b) Han, M.; Michel, R.; He, B.; Chen, Y.-S.; Stalke, D.; John, M.; Clever, G. H. *Angew. Chem. Int. Ed.* **2013**, *52*, 1319-1323; (c) Yamashita, K.-i.; Kawano, M.; Fujita, M. *J. Am. Chem. Soc.* **2007**, *129*, 1850-1851; (d) Kishi, N.; Akita, M.; Kamiya, M.; Hayashi, S.; Hsu, H.-F.; Yoshizawa, M. *J. Am. Chem. Soc.* **2013**, *135*, 12976-12979.

(9) Wang, W.; Wang, Y.-X.; Yang, H.-B. *Chem. Soc. Rev.* **2016**.

(10) (a) Yi, S.; Brega, V.; Captain, B.; Kaifer, A. E. *Chem. Commun.* **2012**, *48*, 10295-10297; (b) Mahata, K.; Frischmann, P. D.; Würthner, F. *J. Am. Chem. Soc.* **2013**, *135*, 15656-15661; (c) Custelcean, R.; Bonnesen, P. V.; Duncan, N. C.; Zhang, X.; Watson, L. A.; Van Berkel, G.; Parson, W. B.; Hay, B. P. *J. Am. Chem. Soc.* **2012**, *134*, 8525-8534; (d) Yan, L.-L.; Tan, C.-H.; Zhang, G.-L.; Zhou, L.-P.; Bünzli, J.-C.; Sun, Q.-F. *J. Am. Chem. Soc.* **2015**, *137*, 8550-8555; (e) Albrecht, M.; Shang, Y.; Rhyssen, T.; Stubenrauch, J.; Winkler, H. D. F.; Schalley, C. A. *Eur. J. Org. Chem.* **2012**, *2012*, 2422-2427; (f) Ren, D.-H.; Qiu, D.; Pang, C.-Y.; Li, Z.; Gu, Z.-G. *Chem. Commun.* **2015**, *51*, 788-791; (g) Jing, X.; He, C.; Yang, Y.; Duan, C. *J. Am. Chem. Soc.* **2015**, *137*, 3967-3974; (h) Wang, Q.-Q.; Day, V. W.; Bowman-James, K. *Angew. Chem. Int. Ed.* **2012**, *51*, 2119-2123.

(11) (a) Tidmarsh, I. S.; Faust, T. B.; Adams, H.; Harding, L. P.; Russo, L.; Clegg, W.; Ward, M. D. *J. Am. Chem. Soc.* **2008**, *130*, 15167-15175; (b) Ramsay, W. J.; Szczypiński, F. T.; Weissman, H.; Ronson, T. K.; Smulders, M. M. J.; Rybtchinski, B.; Nitschke, J. R. *Angew. Chem. Int. Ed.* **2015**, *54*, 5636-5640; (c) Zhou, X.-P.; Liu, J.; Zhan, S.-Z.; Yang, J.-R.; Li, D.; Ng, K.-M.; Sun, R. W.-Y.; Che, C.-M. *J. Am. Chem. Soc.* **2012**, *134*, 8042-8045.

(12) Bell, Z. R.; Jeffery, J. C.; McCleverty, J. A.; Ward, M. D. *Angew. Chem. Int. Ed.* **2002**, *41*, 2515-2518.

(13) Tominaga, M.; Suzuki, K.; Murase, T.; Fujita, M. *J. Am. Chem. Soc.* **2005**, *127*, 11950-11951.

(14) Sun, Q.-F.; Iwasa, J.; Ogawa, D.; Ishido, Y.; Sato, S.; Ozeki, T.; Sei, Y.; Yamaguchi, K.; Fujita, M. *Science* **2010**, *328*, 1144-1147.

(15) (a) Fujita, M.; Nagao, S.; Ogura, K. *J. Am. Chem. Soc.* **1995**, *117*, 1649-1650; (b) Sham, K.-C.; Yiu, S.-M.; Kwong, H.-L. *Inorg. Chem.* **2013**, *52*, 5648-5650; (c) Orhan, E.; Garci, A.; Therrien, B. *Inorg. Chim. Acta* **2015**, *438*, 5-9.

(16) Jentsch, T. J.; Stein, V.; Weinreich, F.; Zdebik, A. A. *Physiol. Rev.* **2002**, *82*, 503-568.

(17) (a) Sakai, N.; Matile, S. *Langmuir* **2013**, *29*, 9031-9040; (b) Vargas Jentzsch, A.; Hennig, A.; Mareda, J.; Matile, S. *Acc. Chem. Res.* **2013**, *46*, 2791-2800; (c) Haynes, C. J. E.; Gale, P. A. *Chem. Commun.* **2011**, *47*, 8203-8209.

(18) L. Caulder, D.; N. Raymond, K. *J. Chem. Soc., Dalton Trans.* **1999**, 1185-1200.

(19) Ronson, T. K.; Zarra, S.; Black, S. P.; Nitschke, J. R. *Chem. Commun.* **2013**, *49*, 2476-2490.

(20) Riddell, I. A.; Smulders, M. M. J.; Clegg, J. K.; Hristova, Y. R.; Breiner, B.; Thoburn, J. D.; Nitschke, J. R. *Nat. Chem.* **2012**, *4*, 751-756.

(21) Dabb, S. L.; Fletcher, N. C. *Dalton Trans.* **2015**, *44*, 4406-4422.

(22) (a) Ma, S.; Smulders, M. M. J.; Hristova, Y. R.; Clegg, J. K.; Ronson, T. K.; Zarra, S.; Nitschke, J. R. *J. Am. Chem. Soc.* **2013**, *135*, 5678-5684; (b) Ousaka, N.; Clegg, J. K.; Nitschke, J. R. *Angew. Chem. Int. Ed.* **2012**, *51*, 1464-1468.

(23) Meng, W.; Clegg, J. K.; Thoburn, J. D.; Nitschke, J. R. *J. Am. Chem. Soc.* **2011**, *133*, 13652-13660.

(24) (a) Pauling, L. *J. Am. Chem. Soc.* **1931**, *53*, 1367-1400; (b) Bondi, A. *J. Phys. Chem.* **1964**, *68*, 441-451.

(25) Campbell, V. E.; Nitschke, J. R. *Synlett* **2008**, *2008*, 3077-3090.

(26) Riddell, I. A.; Hristova, Y. R.; Clegg, J. K.; Wood, C. S.; Breiner, B.; Nitschke, J. R. *J. Am. Chem. Soc.* **2013**, *135*, 2723-2733.
(27) (a) Chifotides, H. T.; Giles, I. D.; Dunbar, K. R. *J. Am. Chem. Soc.* **2013**, *135*, 3039; (b) Chifotides, H. T.; Dunbar, K. R. *Acc. Chem. Res.* **2013**, *46*, 894-906.
(28) (a) Frank, M.; Krause, L.; Herbst-Irmer, R.; Stalke, D.; Clever, G. H. *Dalton Trans.* **2014**, *43*, 4587-4592; (b) Osowska, K.; Miljanić, O. Š. *J. Am. Chem. Soc.* **2011**, *133*, 724-727; (c) Zheng, Y.-R.; Yang, H.-B.; Northrop, B. H.; Ghosh, K.; Stang, P. J. *Inorg. Chem.* **2008**, *47*, 4706-4711; (d) Wu, A.; Isaacs, L. *J. Am. Chem. Soc.* **2003**, *125*, 4831-4835.
(29) Black, S. P.; Wood, D. M.; Schwarz, F. B.; Ronson, T. K.; Holstein, J. J.; Stefankiewicz, A. R.; Schalley, C. A.; Sanders, J. K. M.; Nitschke, J. R. *Chem. Sci.* **2016**, *7*, 2614-2620.
(30) Roberts, D. A.; Pilgrim, B. S.; Cooper, J. D.; Ronson, T. K.; Zarra, S.; Nitschke, J. R. *J. Am. Chem. Soc.* **2015**, *137*, 10068-10071.
(31) (a) Lacour, J.; Ginglinger, C.; Favarger, F.; Torche-Haldimann, S. *Chem. Commun.* **1997**, 2285-2286; (b) Lacour, J.; Moraleda, D. *Chem. Commun.* **2009**, 7073-7089.
(32) (a) Neelakandan, P. P.; Jiménez, A.; Thoburn, J. D.; Nitschke, J. R. *Angew. Chem. Int. Ed.* **2015**, *54*, 14378-14382; (b) Hristova, Y. R.; Smulders, M. M. J.; Clegg, J. K.; Breiner, B.; Nitschke, J. R. *Chem. Sci.* **2011**, *2*, 638-641.
(33) (a) Hammett, L. P. *Chem. Rev.* **1935**, *17*, 125-136; (b) Hansch, C.; Leo, A.; Taft, R. W. *Chem. Rev.* **1991**, *91*, 165-195.
(34) Corey, E. J. *Chem. Soc. Rev.* **1988**, *17*, 111-133.
(35) Baudry, Y.; Bollot, G.; Gorteau, V.; Litvinchuk, S.; Mareda, J.; Nishihara, M.; Pasini, D.; Perret, F.; Ronan, D.; Sakai, N.; Shah, M. R.; Som, A.; Sordé, N.; Talukdar, P.; Tran, D. H.; Matile, S. *Adv. Funct. Mater.* **2006**, *16*, 169-179.

For Table of Contents only

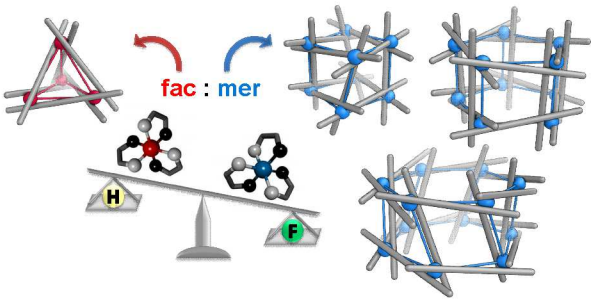

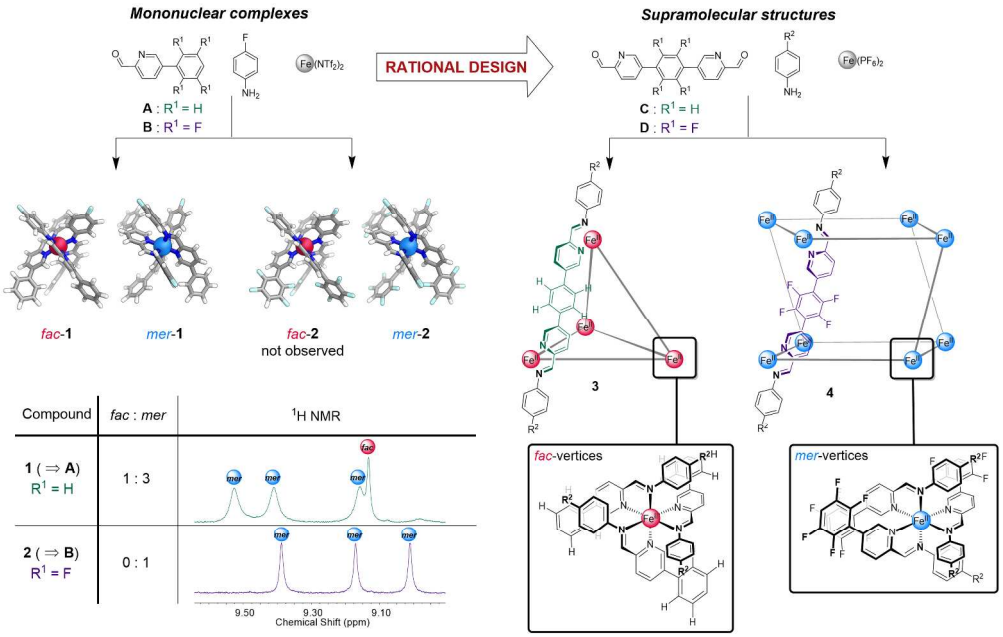

Figure 1. Self-assembly of *fac* and *mer* mononuclear complexes **1** and **2**. ^{1}H NMR spectra (400 MHz, 298 K, CD_3CN) of the imine regions of **1** and **2**. Self-assembly of tetrahedral **3** and tetragonal prismatic **4** from the non-fluorinated **C** and tetrafluorinated **D** subcomponents respectively.
369x232mm (192 x 192 DPI)

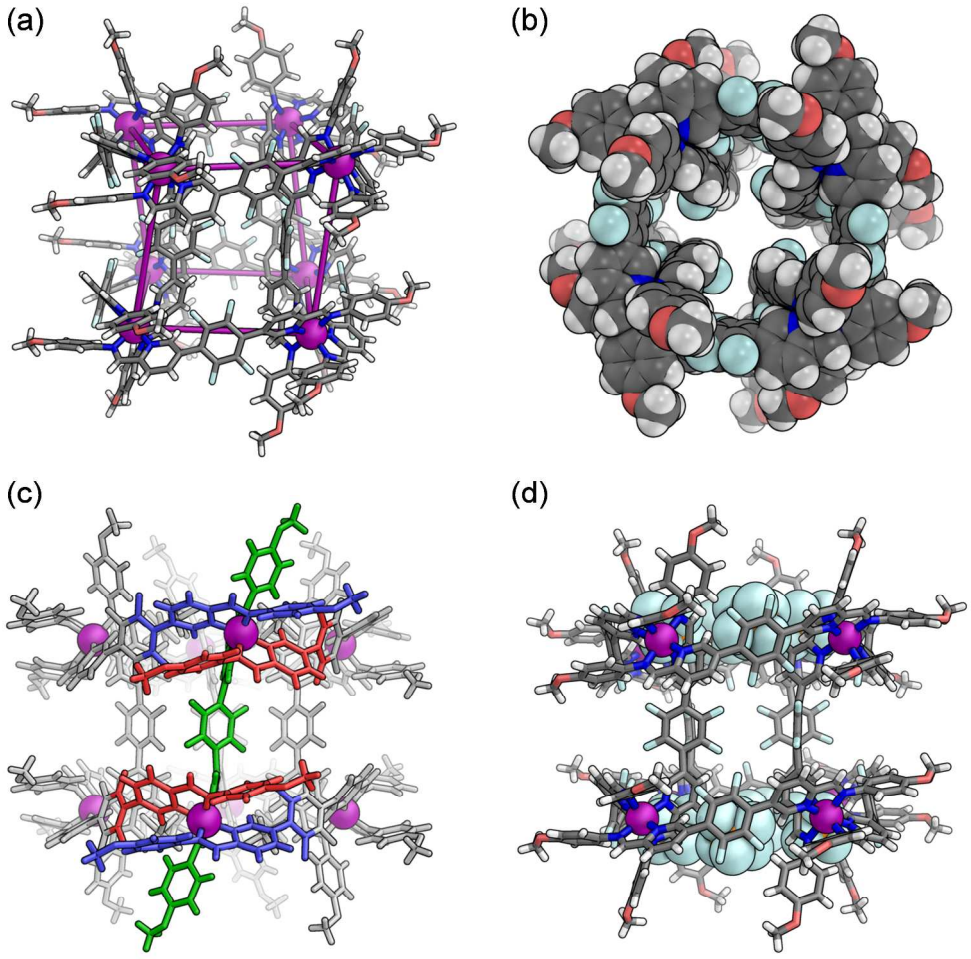

Figure 2. Views of the single crystal X-ray structure of **4a** (a) showing the top and bottom rings linked by axial ligands, with linkages between Fe^{II} centers (purple spheres) added in order to highlight the D_4 point symmetry; (b) showing the ligands in a space-filling view down the central channel; (c) highlighting a pair of *mer* vertices, with the three magnetically distinct environments shown in blue, red, and green; (d) showing the placement of the ordered PF_6^- counterions above the -C_6F_4- rings. In all views the non-encapsulated anions, solvent molecules and disorder are omitted for clarity.
564x565mm (192 x 192 DPI)

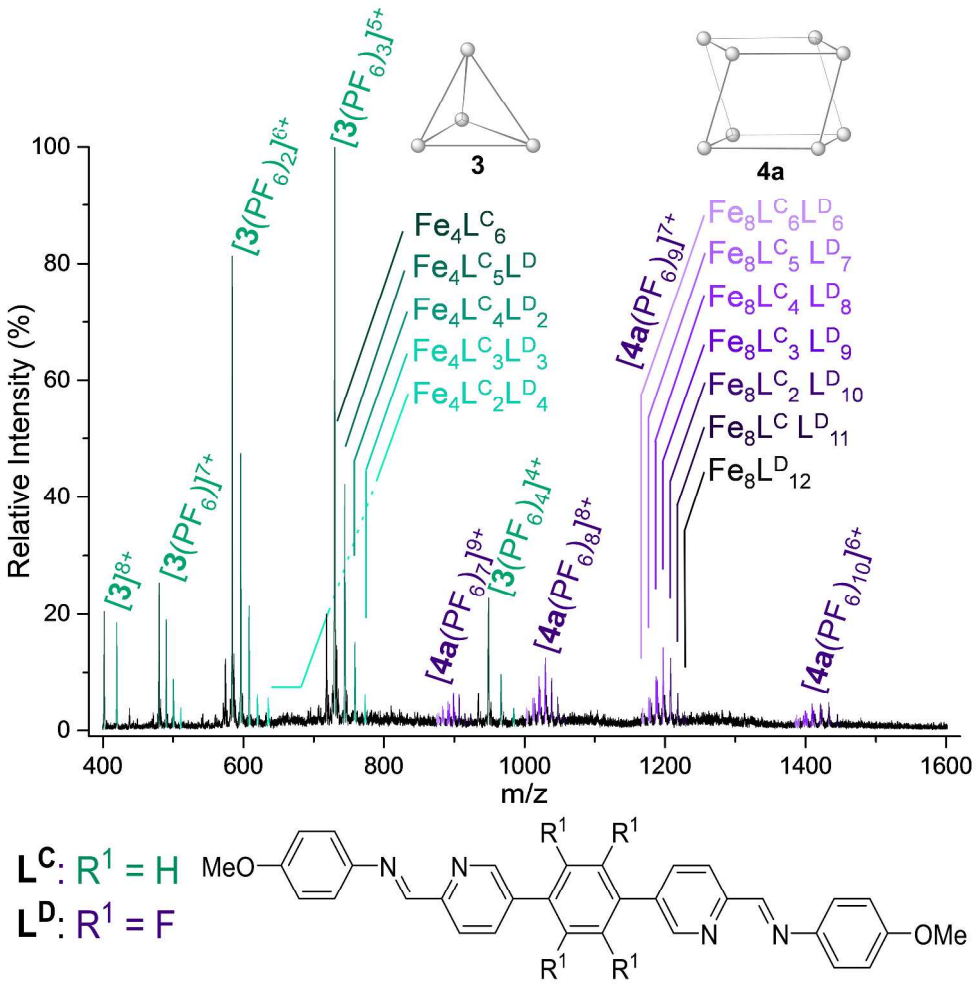

Figure 3. ESI-MS of a mixture of preformed structures **3** and **4a** in a 2:1 ratio after equilibration at 50 °C for one week.
604x594mm (192 x 192 DPI)

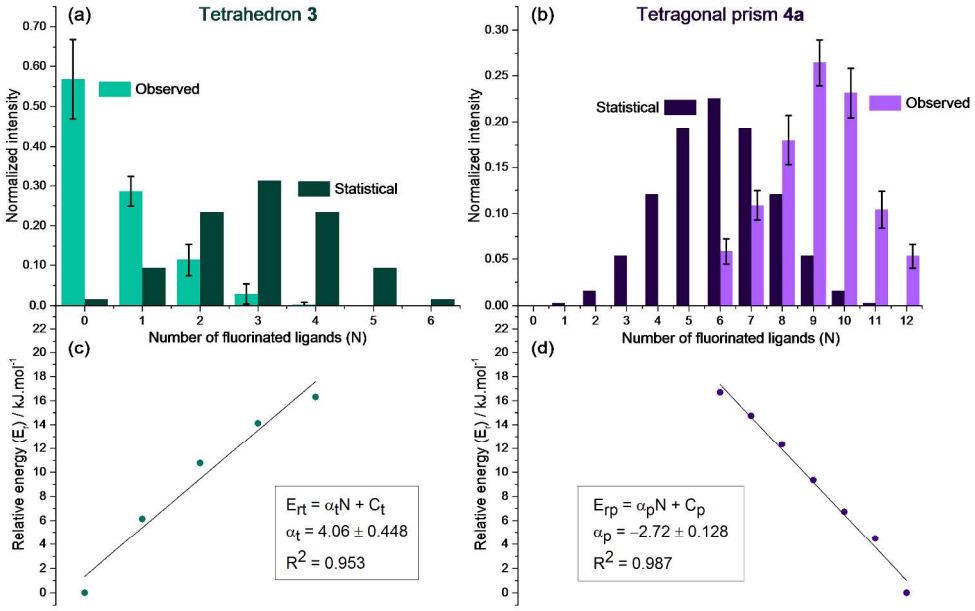

Figure 4. Proportion of each species observed for (a) tetrahedron **3** and (b) tetragonal prism **4a** compared to the binomial (statistical) distribution. Error bars represent the standard deviations of the amounts of each congener measured between the different charge states observed in the ESI-MS. (c) and (d) provide plots of the energy of each species relative to tetrahedron **3** in (c), containing only non-fluorinated **C** residues, and the tetragonal prism **4a** in (d), containing only fluorinated **D** residues. E_{rt} and E_{rp} refer to the relative energies between congeners respectively in the cases of the tetrahedral series and the prismatic series. α represents the energetic destabilization per ligand exchanged.
393x262mm (192 x 192 DPI)

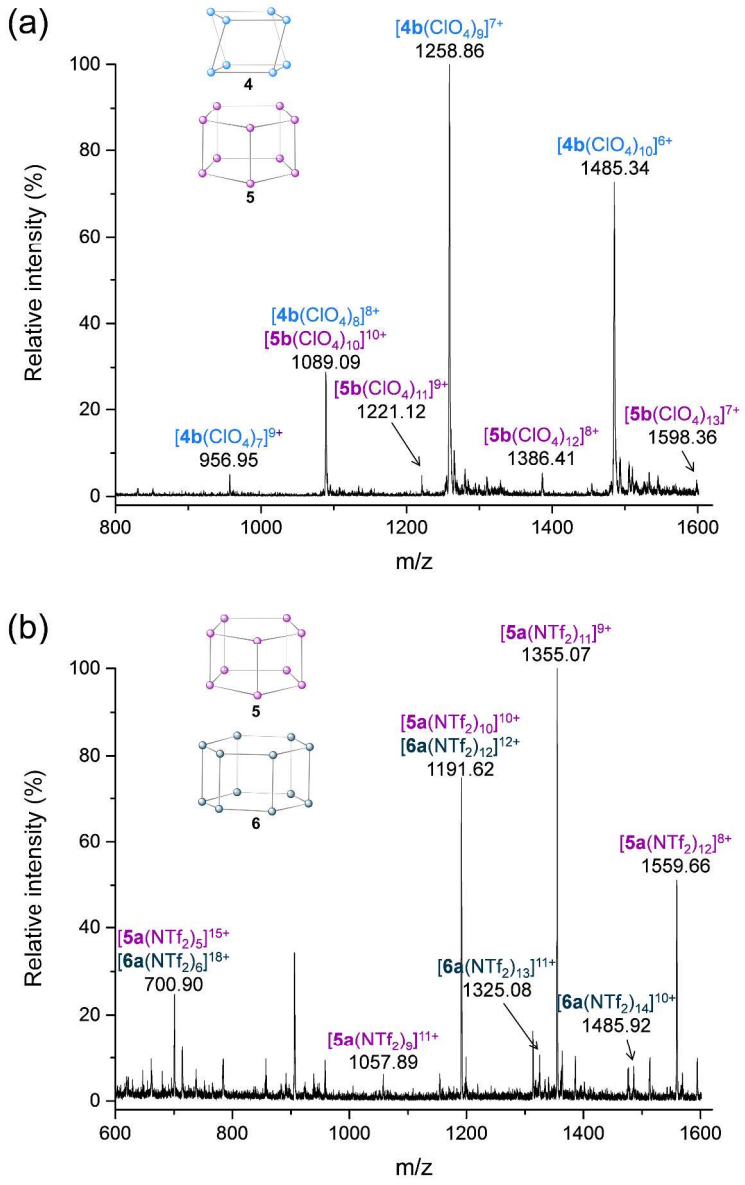

Figure 5. ESI-MS of a mixture of (a) **4b** and **5b** and (b) **5a** and **6a**.
654x1034mm (192 x 192 DPI)

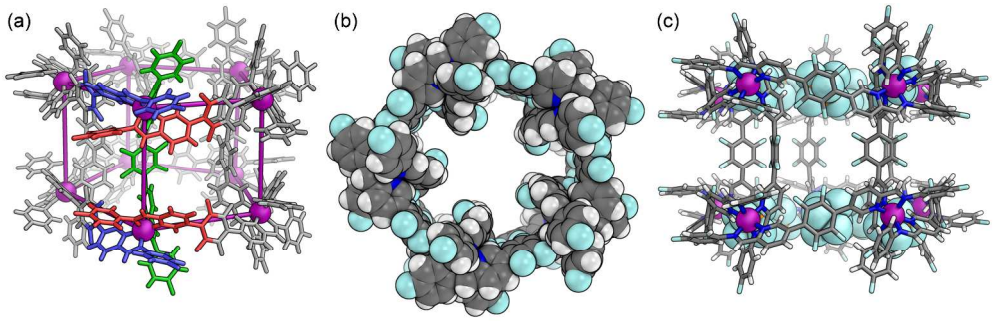

Figure 6. Single crystal X-ray structure of **5c** showing (a) the two pentagonal faces linked by axial ligands, with connections between metal centers (purple spheres) added to highlight the C_{5h} point symmetry; (b) spacefilling view down the central channel; (c) side view showing the specific positions of the localized PF_6^- counterions. In all views the non-encapsulated anions, solvent molecules and disorder are omitted for clarity.
793x261mm (192 x 192 DPI)

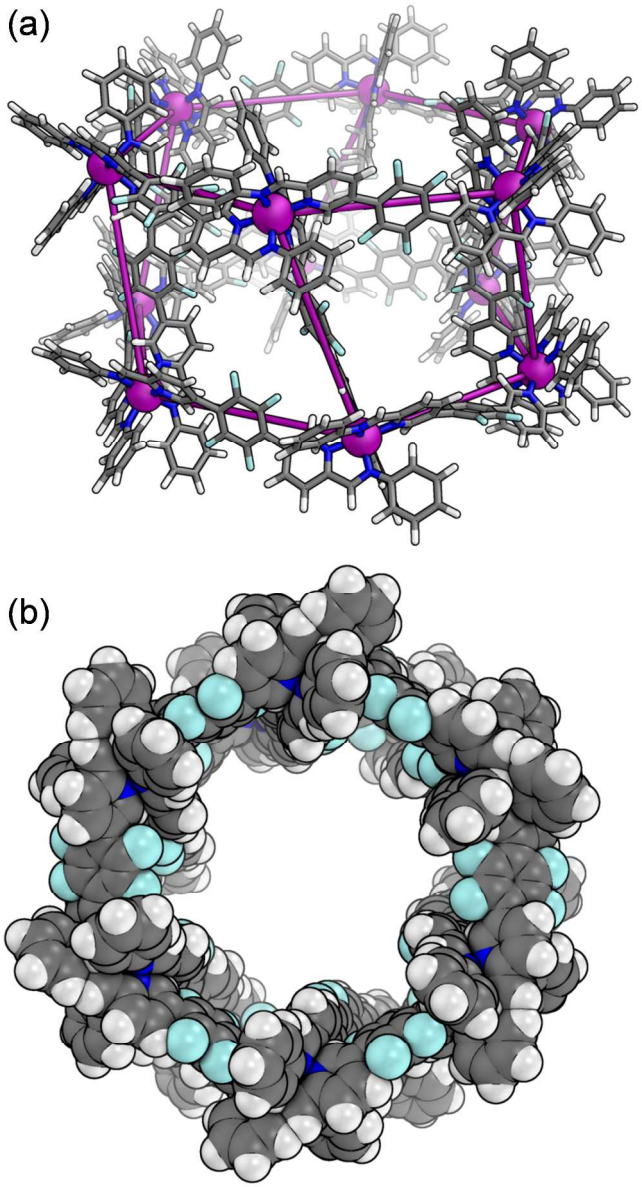

Figure 7. (a) MM3-optimized molecular model of hexagonal prism **6h** (R=H). Connections between metal centers (purple spheres) have been added to highlight the D_6 point symmetry; (b) spacefilling view down the central channel. No anions were modeled.
327x594mm (192 x 192 DPI)

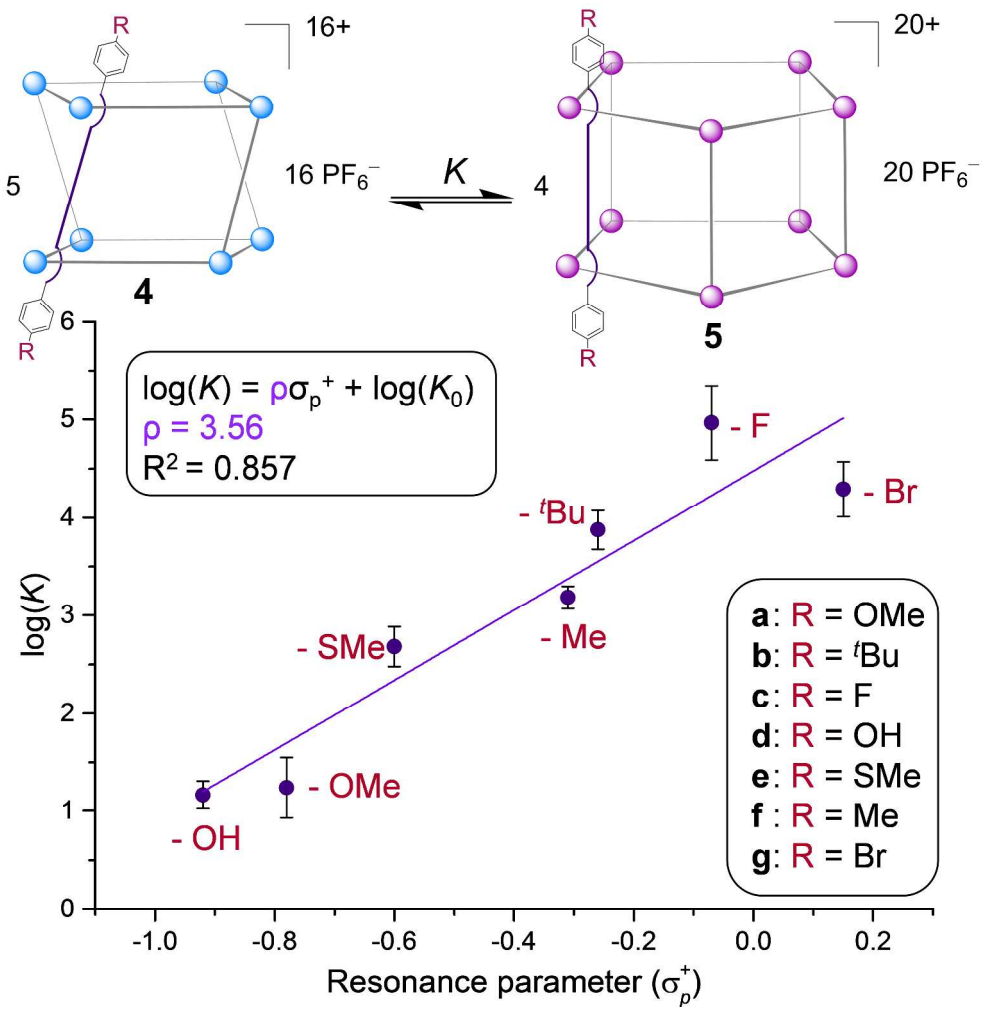

Figure 8. Equilibria between **4** and **5** show a linear free energy relationship between log(*K*) and σ_p^+, following the Hammett Equation. The error bars show standard deviations of log(*K*) over 5 runs.
593x594mm (192 x 192 DPI)

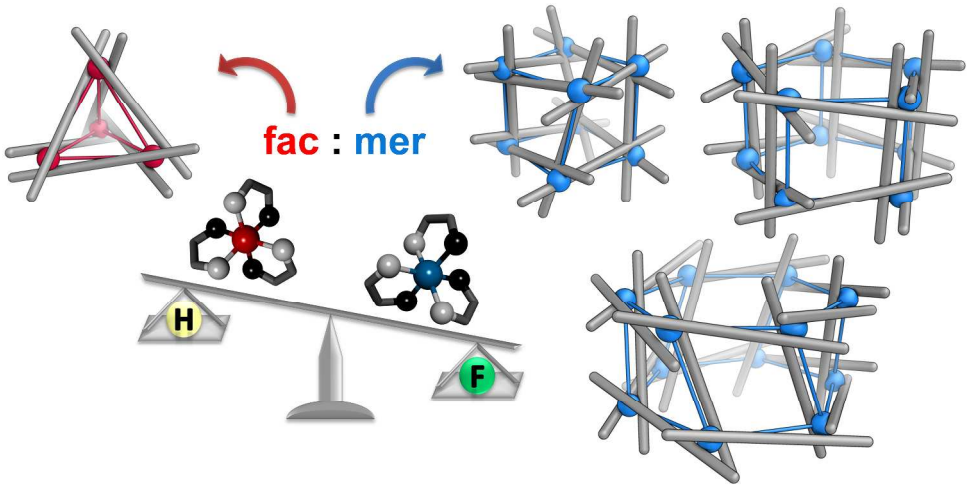

793x393mm (192 x 192 DPI)